TRANSACTIONS OF THE INSTITUTE OF MEASUREMENT & CONTROL

Article

Transactions of the Institute of Measurement and Control
2015, Vol. 37(4) 522–535

DOI: 10.1177/0142331214543299
tim.sagepub.com
SAGE

Image processing assisted locomotion observation of cockroach *Blaptica Dubia*

Xingming Wu[1], Dong Liu[1], Weihai Chen[1], Jianhua Wang[1], Shaoping Bai[2], Zhifeng Li[1] and Guanjiao Ren[1]

Abstract

High-speed camera recordings are very useful for analysis of animal behaviors. However, in earlier studies, the analysis has to be conducted by manually extracting data from video, which is not only time-consuming but also subjective. In this work, we developed a new method of movement tracking for an easy locomotion observation, and applied this method to the motion analysis of the cockroach, *Blaptica Dubia*. Image processing algorithms were developed to extract information of points of interest on cockroaches, which was implemented in two steps: identification and tracking. With the developed method, experiments were conducted focusing mainly on velocity, gait and stability. The results showed the feasibility of the new method for more intensive locomotion observation with applications in walking robots.

Keywords

Cockroach, identification, image processing, locomotion observation, movement tracking, walking robots

Introduction

The study of animal and human locomotion behaviors has been a classical topic for many years. An early study can be dated back to 1870s, when Eadweard Muybridge recorded the motion of a horse by photography, and studied the trot gait and gallop gait of the horse (Clegg, 2007). In the 1950s, films at a speed of 16–32 frames per second (fps) were used by GM Hughes to study insects' morphology and kinematics (Hughes, 1952). With similar optical equipment and methods, extensive investigations were carried out on different kinds of species such as human, medusa, limpet, and cockroach (Daniel, 1985; Delcomyn, 1971; Moeslund et al., 2006). In the meantime, mechanical equipment such as treadmill and force-platform were used to study biomechanics, dynamics and energetics of creature locomotion (Fukunaga et al., 2001; Jindrich and Full, 2002; Holmes et al., 2006).

Up to date, technology advances have made high-speed cameras widely available for the study of animal locomotion (Hermanson, 2004; Cruse and Bartling, 1995; Dickinson et al., 2000; Höfling and Renous, 2004). Moreover, by combining several high-speed cameras, it is possible to capture the three-dimensional movements of creatures, which can provide more comprehensive and accurate data for analysis (Drucker and Lauder, 2000; Hsieh, 2003; Ritzmann et al., 2004). With abundant experimental information obtained, hypotheses were verified and tested, such as the central pattern generators (CPGs) in insects and models for legged locomotion (e.g., inverted pendulum for walking and spring-mass model for running) on multi-legged creatures (Cruse, 2002; Ijspeert, 2008; Kuo, 2002). Models and rules extracted from experiment analysis and results have been used in other fields such as bio-inspired robots (Altendorfer et al., 2001; Garcia et al., 2007; Quinn et al., 2003). However, for most applications of the high-speed camera, the points of interest in records were identified by manual operations. Therefore, not only is the operation time-consuming and tedious, but the data is also subjective and contains some uncertain deviation.

The advanced computer vision and image processing technology today offers new opportunities and techniques to ease the analysis of high-speed camera recording. A well-known application is the human motion capture in the gaming and film industries, where reflective or luminous markers are placed on the skin of a human subject to establish brief models of the subject (Cappozzo et al., 2005; Chan et al., 2011). However, for small subjects (such as insects), the reflective or luminous markers are too big to be placed on places of interests such as leg-ends, so vision and image techniques can only be used for kinematics analysis of the whole goals or main parts of body in earlier studies (Bai et al., 2000; Fontaine et al., 2009; Spence et al., 2010).

[1]School of Automation Science and Electrical Engineering, Beihang University, Beijing, China
[2]Department of Mechanical and Manufacturing Engineering, Aalborg University, Denmark

Corresponding author:
Weihai Chen, School of Automation Science and Electrical Engineering, Beihang University, No. 37, Xueyuan Road, Haidian District, Beijing 100191, China.
Email: whchenbuaa@126.com

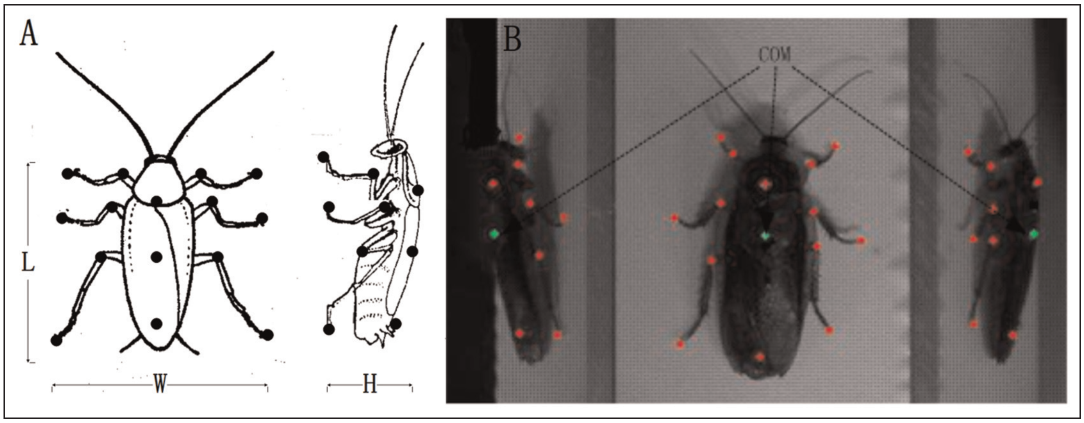

Figure 1. (A) The positions of mark points on the cockroach. The black dots on the body and legs indicate the points of interests. (B) An image of a subject captured by the camera, where all points of interest are shown in red, except the COM in green.

In this work, an experimental platform was designed to obtain efficiently and conveniently the locomotive information of a cockroach. Image processing algorithms were applied to identify and track the points of interests on the specimen. In particular, the algorithm is able to track the movement of points on legs, along with the body points, to provide us the information of locomotion at insect-leg level. Moreover, the motion was captured in three-dimensional space by virtue of one camera only. With the developed method, analysis was conducted with focus on the moving velocity and animal gaits. Some of the observation results and movement rules discovered have been applied to the design and control of walking hexapod machines.

Materials and methods

Animals/specimen

The subjects of investigation are adult female cockroaches, *Blaptica Dubia*. In total, 47 cockroaches were used, which ensures significance of statistics. The average dimensions of the subject specimens are $L = 38$mm, $W = 22$ mm, $H = 12$mm, where L, W, H represent the length, width, and height, respectively, as shown in Figure 1(A). All the cockroaches were intact and wholesome during the experiments.

In order to track clearly the motion of body parts, we painted the cockroaches on selected points. We used white paint for a high contrast to the body image of the cockroach. The points of interests include the center of mass (COM), two points on the central axis of body, leg-ends and femur-tibia joints of six legs, as shown in Figure 1(B). With these key points, a brief model can be constructed to describe 3D locomotion of the cockroaches.

Experimental platform

An experimental platform, as shown in Figure 2, was constructed for locomotion observation of cockroaches. This platform is essentially a locomotion tracking system, made up of a motion capture module and a data processing module.

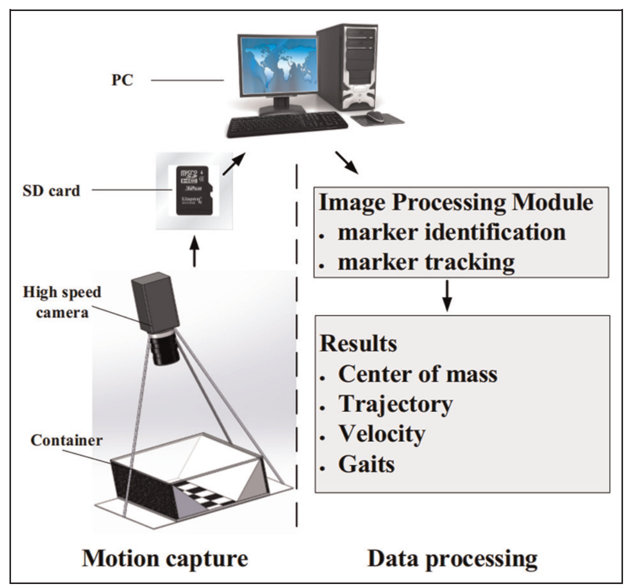

Figure 2. Sketch of the experimental platform for locomotion observation.

The motion capture module includes a high-speed camera, a perspex container, two mirrors, artificial terrains, a data recorder (SD card), and a PC. The high-speed camera, IGV-B0620C, is placed on top of the container and orientated towards the terrain. It records at a speed of 260 fps with a resolution of 648 × 488 pixels. The size of the container where the cockroach movement is observed measures 30 × 20 × 10 cm. Two mirrors are placed at two flanks of the specimens, so that each frame contains three views of cockroaches. With at least two views of a point, three-dimensional coordinates of the selected points could be obtained. Artificial terrain is located between two mirrors to provide the environment for cockroach locomotion. All the measurements were conducted in the evening, the most active circadian phase of cockroaches. This measuring equipment was emplaced indoors where temperature and humidity are nearly stable. The temperature was 20 ~ 25°C and the humidity was 40 ~ 60%. Lighting was controlled with two incandescent bulbs (150 W), placed over each end of the platform. The light intensity was regulated to below 1,500 Lux, to reduce injuries to the specimens.

In the experiments, only one cockroach at a time was placed in the starting end of the container, and they were left there for one minute to adapt to the new environment. During the observation break between two cockroaches, the floor of the container was washed with detergent and water to remove any physical or chemical evidences of previous occupants. The light was turned off periodically during the photographic sessions to avoid habituation of cockroaches. The visual field of the camera is about 20 × 15 cm. Providing that the image resolution of the camera is 648 × 488 pixels, the real-world resolution is approximately 3 pixels / mm, which is enough to reach satisfying results with the help of the painted markers.

Mathematical model

As one camera can only obtain two-dimensional information of the marker points, virtual stereo vision system was used here to provide extra information for determination of three-dimensional coordinates of the cockroach body (Wang et al., 2009). The real point and corresponding reflect point in mirrors can provide at least double two-dimensional information of one marker point. In Figure 3(A), a front view model is presented to show the motion capture system. In order to simplify computing, the geometric center of the object observation region was set as the origin of the world coordinate system. The high-speed camera was placed vertically and the height was adjusted to obtain proper vision field. The camera was located at $C(0, 0, \mathrm{h})$, and its projection on objective plane was defined as the origin of the world coordinate system. While mark point $P(x, y, z)$ was captured by the camera, a reflected point $P_1(x_1, y_1, z_1)$ would be generated by the mirror, just like that another camera captured point C from the left side. As mirrors were mounted parallel to the y axis, the position of virtual camera at the left side could be defined as $C_1(c_1, 0, d_1)$. Points $Q(u, v)$ and $Q_1(u_1, v_1)$, which represented P and P_1, respectively, in frame plane, were measured in pixels.

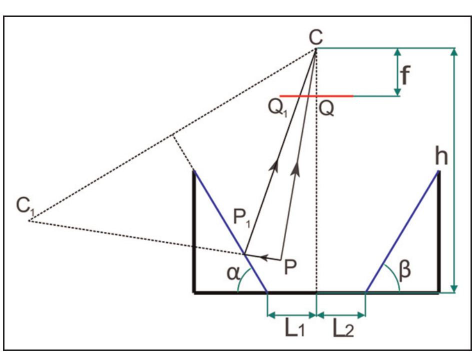

Figure 3. Mathematical model of the platform. The blue lines stand for the mirrors, the red line stands for the image plane. Pinhole camera geometry is used here to model the experimental platform.

Parameters h (the z coordinate of point C) and focal length f could be obtained through camera calibration, and other parameters such as α, β, L_1, L_2 could be measured directly on experimental platform. With these parameters, coordinate of mark point P could be expressed as:

$$\begin{cases} x = \dfrac{-2uv_1 \tan\alpha(\mathrm{h} + L_1 \tan\alpha)}{uv_1 - u_1 v + uv_1 \tan^2\alpha + u_1 v \tan^2\alpha - 2vf \tan\alpha} \\ y = \dfrac{-2vv_1 \tan\alpha(\mathrm{h} + L_1 \tan\alpha)}{uv_1 - u_1 v + uv_1 \tan^2\alpha + u_1 v \tan^2\alpha - 2vf \tan\alpha} \\ z = h - \dfrac{2v_1 f \tan\alpha(\mathrm{h} + L_1 \tan\alpha)}{uv_1 - u_1 v + uv_1 \tan^2\alpha + u_1 v \tan^2\alpha - 2vf \tan\alpha} \end{cases} \tag{1}$$

If point P was located at the right side, its coordinates were calculated by

$$\begin{cases} x = \dfrac{2uv_1 \tan\beta(\mathrm{h} + L_2 \tan\beta)}{uv_1 - u_1 v + uv_1 \tan^2\beta + u_1 v \tan^2\beta - 2vf \tan\beta} \\ y = \dfrac{2vv_1 \tan\beta(\mathrm{h} + L_2 \tan\beta)}{uv_1 - u_1 v + uv_1 \tan^2\beta + u_1 v \tan^2\beta - 2vf \tan\beta} \\ z = h - \dfrac{2v_1 f \tan\beta(\mathrm{h} + L_2 \tan\beta)}{uv_1 - u_1 v + uv_1 \tan^2\beta + u_1 v \tan^2\beta - 2vf \tan\beta} \end{cases} \tag{2}$$

Prior to each experiment, the camera had to be adjusted slightly to obtain clear images. The camera was calibrated to establish a mapping relationship between the world coordinate system and the digital image.

Markers identification and tracking

An image processing algorithm was developed to process the records, such that most of the work could be executed by a computer program automatically. The image processing algorithm was conducted in two steps: marker identification in a single frame, and marker tracking between two adjacent frames.

Marker identification. Marker identification is to extract the two-dimensional coordinates of the markers in a frame. In order to describe the locomotion of cockroaches in a series of frames, markers on cockroaches should be recognized and extracted in their own frame.

Figure 4(A) shows the flow chart of image processing for marker identification. At the first step, initialization was manually performed on the first frame of a sequence, and blobs were drawn for each marker at a size of about 15 × 15 pixels. This initial process simplifies the identification from the whole image to several boxes, which not only reduces the workload of image processing, but also improves the reliability of marker identification. In the initialization, all points were registered with respect to the point selection shown in Figure 1.

Following the initialization, mark points are further identified by the algorithm. The markers were divided into two types according to their size: leg-end markers and body markers. For the leg-end markers, the size was always several pixels, and the shape character of legs was remarkable within boxes. The Harris corner detection method was used to

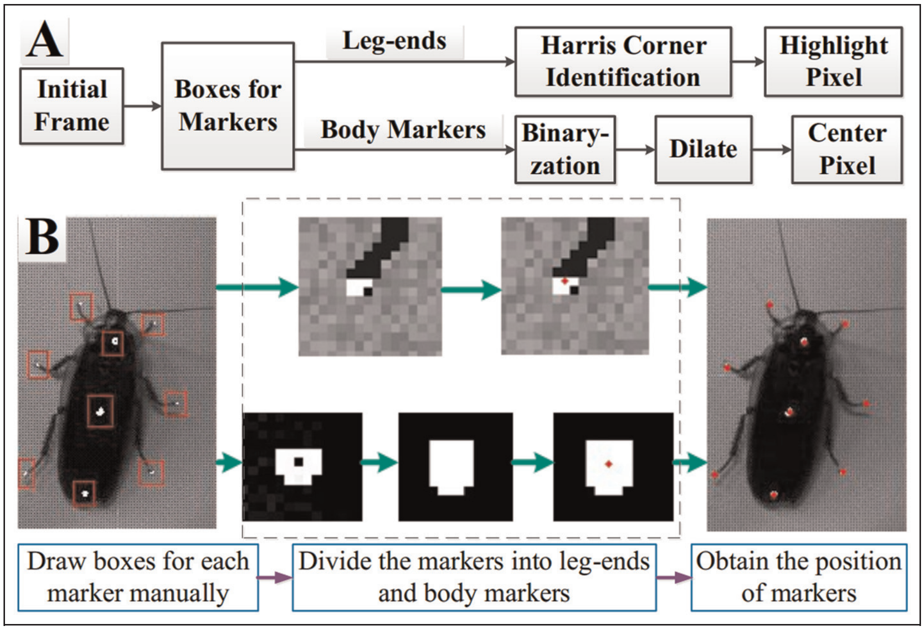

Figure 4. (A) Flowchart of the marker identification. (B) The graphic illustration.

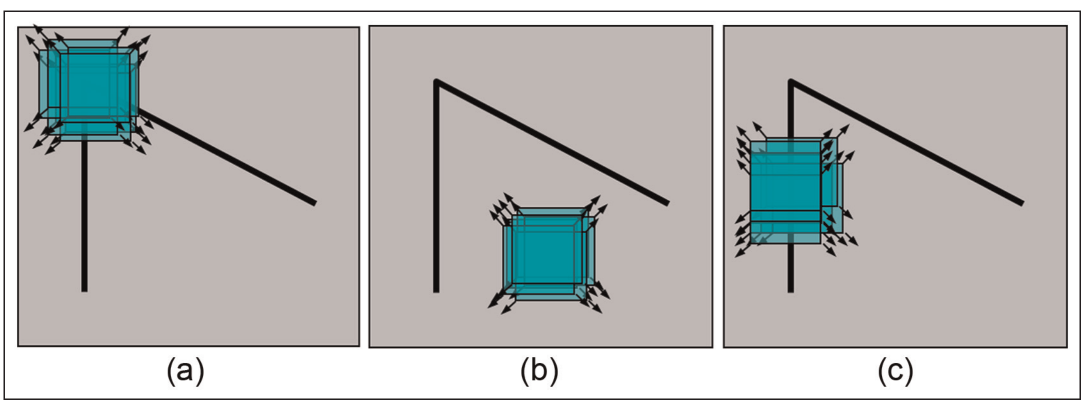

Figure 5. Illustration of (a) corner area, (b) flat area, and (c) edge area.

identify leg-ends within these boxes (Harris and Stephens, 1988), under the consideration that pixels with large Harris values are always distributed around the leg-end and can thus be extracted. The Harris corner detection method is described as follows.

The basic principle of the Harris detection is to inspect the changes of gray value in a window, after the local window centered with the target pixel makes a new offset in different directions. We divided the images into three areas, as shown in Figure 5: a) corner area where a big change of gray value in both horizontal and vertical directions; b) flat area where the changes of gray value in both horizontal and vertical directions are small; c) edge area, where a big change of gray value in either horizontal or vertical direction is identified.

For a small window centered with pixel (m, n) moving along x-axis by u and y-axis by v, the change of gray value $E_{\mathrm{m,n}}$ is given by

$$E_{m.n} \cong [u, v] M \begin{bmatrix} u \\ v \end{bmatrix} \tag{3}$$

where matrix M is a real symmetric matrix, obtained by

$$M = \sum_{m,n} w_{m,\mathrm{n}} \begin{bmatrix} I_m^2 & I_m I_n \\ I_m I_n & I_n^2 \end{bmatrix} \tag{4}$$

where $w_{m,\mathrm{n}}$ is a window function, usually defined as $w_{m,\mathrm{n}} = e^{(m^2+n^2)/\sigma^2}$, and I is the image gray value function. After the diagonalizing process, equation (3) becomes

$$E_{m,n} = R^{-1} \begin{pmatrix} \lambda_1 & 0 \\ 0 & \lambda_2 \end{pmatrix} R \tag{5}$$

where R is twiddle factor, and λ_1, λ_2 are eigenvalues. Corner response function *CRF* is obtained as

$$CRF(x, y) = \det(M) - k(\mathrm{trace}(M))^2 \quad (0.04 < k < 0.06) \tag{6}$$

where $\det(M) = \lambda_1\lambda_2$ is the determinant of M, and $\mathrm{trace}(M) = \lambda_1 + \lambda_2$ is the trace of M.

If the *CRF* of target pixel is larger than a given threshold, the pixel is detected as a corner.

The Harris corner detector has a number of advantages including simple calculation, uniform and reasonable extraction of point features, and high stability, etc. The limits of the Harris operator are that it is sensitive to scale and the extracted corner is pixel level. In practice, gray values were also used to verify the marked pixel, the pixel with larger Harris value and gray value would be considered as the position of the marker point. As a result, the leg-end markers were identified as the highlight pixels.

For the body markers, gray value threshold criterion was used to carry out the identification. Since the body markers occupy 30 pixels in the image, the geometric center of the painted area has to be extracted in order to reduce the deviation. First, the p-parametric method was used in the binarization process, which is the central step. Suppose the proportion of target area is p_1 in image distribution histograms $p(t)$, and t is image grey value, where $t = 0, 1, 2, \ldots, 255$. The cumulative distribution histogram of the image is given by

$$p_1(t) = \sum_{i=0}^{t} p(i) \tag{7}$$

The threshold value T is calculated by

$$T = \arg\min|p_1(t) - \mathrm{p}_1| \tag{8}$$

The image binarization is realized according to the threshold value. With the binarization being extended to the marked areas (white areas), all pixels in the whole area are connected. Finally, the geometric center is calculated to obtain the coordinates of the mark points. As shown in Figure 5(B), an image is firstly binarized to identify mark pixels with others in a box. Then image dilating and eroding process are performed to make the marker an integrated zone, such that the center pixel could be calculated by averaging and rounding all the white pixels coordinates. As a result, the body markers are identified as the center pixels.

Marker tracking. With the aforementioned algorithm, all the markers were identified in the initial frame. Next, we need to determine these markers' correlations from one frame to the next. Frame differencing method was applied here, which was realized by computing pixel differences among several contiguous frames (Yin et al., 2011). In our method, differences between two frames were calculated to divide the markers into two groups: moving and stationary markers. The stationary markers pertain to the leg-end in supporting phase, while the moving markers correspond to the points on the main body and the points on leg joints. As shown in Figure 6(A), subtracting a pixel's gray value of the former frame from present frame, the gray values of stationary leg-end markers are almost zero because the positions do not change in two sequential frames. Therefore, we consider that the two-dimensional coordinates are the same in two images. However, for moving markers, as the position of marked points change, the gray values of corresponding zones are different in two frames. As shown in the middle image of Figure 6(B), the white parts show the differences between two images. To be specific, differential calculation of two adjacent frames in video sequences accomplishes as the first step, as shown in equation (9)

$$D_k(x, y) = |I_{k+1}(x, y) - I_k(x, y)| \tag{9}$$

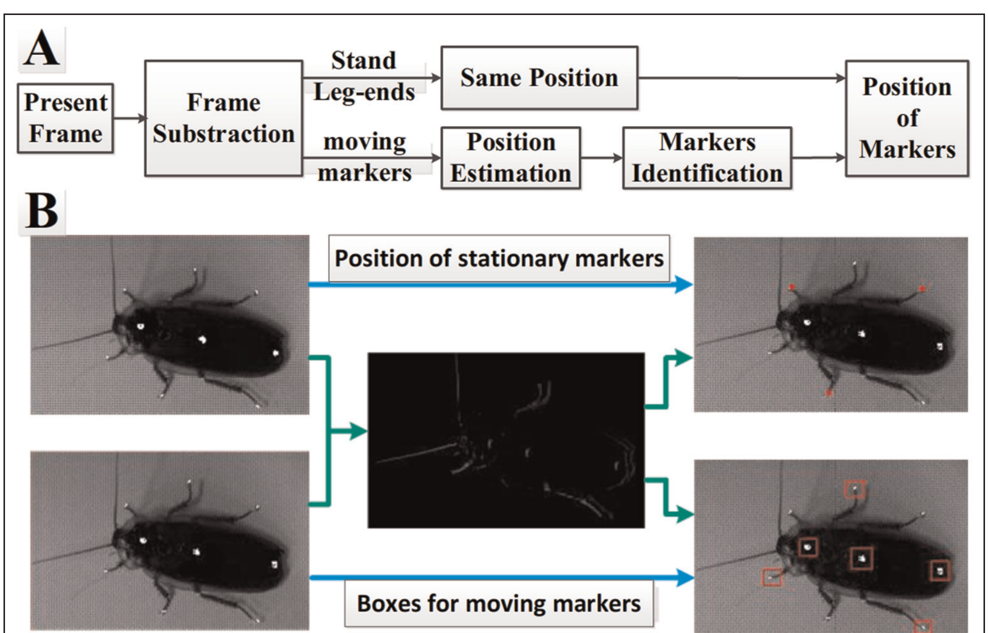

Figure 6. (A) Flowchart of the markers tracking. (B) Graphic illustration of marker tracking for stationary and moving markers.

where, $D_k(x,y)$, $I_k(x,y)$ and $I_{k+1}(x,y)$ are differential image, the current frame and the next frame, respectively. The threshold segmentation is completed with:

$$T_k(x,y) = \begin{cases} 0, & D_k(x,y) < T \\ 1, & D_k(x,y) \geq T \end{cases} \tag{10}$$

where, $T_k(x,y)$ and T are foreground image and threshold segmentation, respectively.

However, it was found that some vacancy appeared when detecting the target images with frame differencing method. As the swing leg-ends and body markers were moving, the boxes in former frame might not be properly identified for each marker in present frame, which means new boxes should be plotted. In this light, position estimation method was used here to make a priori estimate about zones of boxes. Through the roughly observation of cockroach movements, we could find that: 1) the cockroaches moved forward, not backward, 2) unless coming to obstacles, the cockroaches went nearly straight forward. With the a priori knowledge, we could achieve more feasible and accurate estimates. For body markers, from the displacement of a marker in two sequential frames, we firstly made an estimated position of a mark point in *i*-th frame based on the mark position in (*i*-1) th and (*i*-2) th frames. A box was then plotted at a size of 20 $\times$ 20 pixels, whose center was the estimated mark point. The marker identification would be taken within this box to obtain the final position of the mark point. For swing leg-ends, as the range of the displacement was bigger in both x and y axes, the priori estimation was more complicated. After the position of the COM in present frame was obtained, we took the vector of the COM between former frame and present frame as the moving orientation of the leg-ends, and the mean value of two former displacements of corresponding leg-end as the present displacement. With the orientation and displacement, the estimated position of leg-end was obtained.

The algorithm is able to process images at a speed of 0.8 s / frame on a low-end hardware (32-bit Intel Dual-Core i3-2130 CPU @ 3.40G Hz and DDR3 – 4GB memory), which is acceptable in this work. Note that the processing speed of the algorithm is subject to on the configuration of computers. As the proposed image processing algorithm is actually a hybrid method combining both manual and automatic processes, a major effort in further development will be on how to minimize the effort in the initialization handled by human. The average tracking error relative to manual extraction is less than 1 mm. It is noted that some of the tracking errors come from the procedures of image processing, e.g., filtering processing in marker identification. While the algorithm can be improved further, the current accuracy is sufficient for motion tracking of cockroaches.

Results of locomotion observation

Experiments were carried out on flat solid surfaces. All segments of continuous movements were selected as samples, which included 9 different sequences (about 50 strides). A total of 2,085 frames were processed in each measurement to support the following analysis.

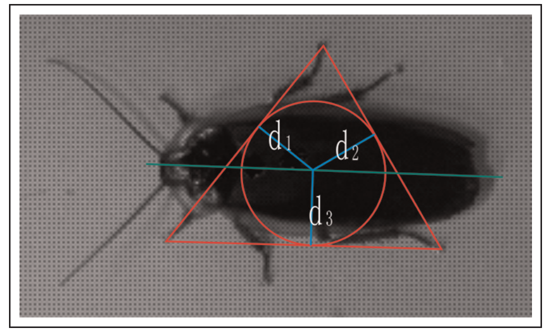

Figure 7. Position of the COM of cockroach. The green line shows the center line of cockroach, the red lines show the support triangle and its inscribed circle, the blue lines show distances between the COM and edges of support triangle.

Center of mass

We studied first the COM. The theory of stability margin (d) (the shortest distance from the center of gravity to the boundaries of support triangle) was used here to get the position of the COM (Hof et al., 2005; Lafond et al., 2004). The cockroaches were filmed in a static relaxed stance, as shown in Figure 7, with all the legs being outstretched. The support triangle and the center line of the cockroaches were drawn. As the COM must locate on the center line, the COM could be determined by maximizing the stability margin ($d_1 = d_2$). The ideal center of stability (ICS) is relevant to stability margin, which is also used to assess the stability of moving specimen (Ting et al., 1994). We recall that the ideal center of stability is defined as the center of inscribed circle of support triangle ($d_1 = d_2 = d_3$). When the COM coincides with the ideal center, stability margin is the largest. Distance between the COM and the ideal center of stability can be used to assess the stability. The shorter the distance is, the better the stability of the cockroach.

Trajectories of the leg-ends and the COM were shown in Figure 8(A), where all footprints of leg-ends were extracted and displayed in Figure 8(B). Based on these points, all support triangles and corresponding centers can be identified. From the distribution of trajectories, we can find that the COM is always located between two adjacent supporting tripods with almost the same distance. It means that stability margin of the assumed COM is almost the maximum during locomotion, and the position of the assumed COM was almost coincident to the ideal center of stability.

Trajectories of leg-ends

The new method allows us to obtain the three-dimensional trajectories of legs. Considering the symmetrical characteristic of stick animals, we looked at the three-dimensional trajectories of left leg-ends only. Figure 9 shows the trajectory of cockroach walking along the x axis. It can be observed that the step length of every walk is equal for all legs, while step heights are obviously different, as shown in Figure 10. Further measurements give that the step heights are about 9.7mm, 5.8mm, and 3.9mm for the front, middle, and hind legs, rspectively.

Velocity

Velocity is the variable that can show kinematic performance directly. In our analysis, we looked at both instantaneous and average velocities. In our experiments, instantaneous velocity was calculated by dividing distance of the COM between the former one and the latter one by 10ms (the camera configuration was 200 fps, so the interval of two adjacent frames was 5ms). Mean stride velocity is defined as the average speed of the cockroach in a stride, which is calculated by dividing displacement of the COM by the duration time of a stride.

Figure 11(A) shows the instantaneous velocity for nine sequences, which were smoothly processed to avoid abrupt change. The mean stride velocities of each sequence were shown in Figure 11(B). In our trials, when cockroaches moved on flat terrain with a continuous velocity, the velocity ranges from 3 to 23 $cm\ s^{-1}$. Moreover, the corresponding mean stride velocity ranges from 6 to 20 $cm\ s^{-1}$, the average velocity being 11.37±3.2 $cm\ s^{-1}$ for the 47 subjects as a whole.

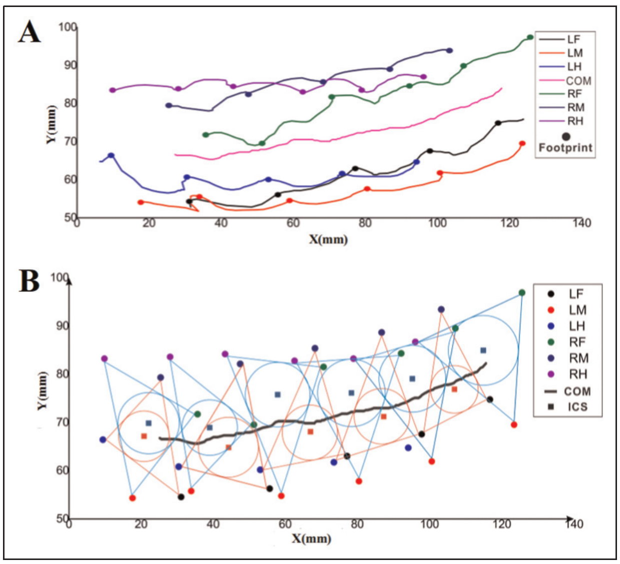

Figure 8. Verifying the position of the COM. (A) Trajectories of leg-ends and the COM of cockroach at horizontal plane, where all dots stand for footprints. (B) Supporting triangles and ideal centers of stability (ICS, indicated by small solid squares).

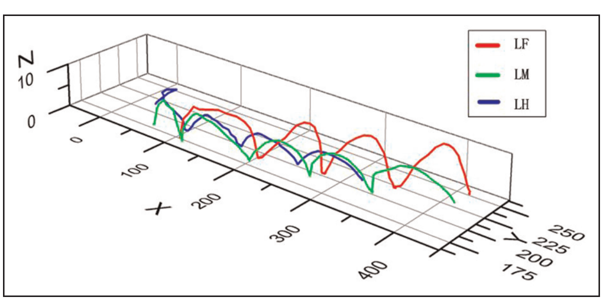

Figure 9. Three-dimensional trajectories of three leg-ends (left front leg (LF), left middle leg (LM), left hind leg (LH)) of cockroach walking on flat terrain (x and y axes unit: pixel; z axis unit: mm).

Movement of an individual leg

Duty factor is one of the most important variables to describe strides, defined as the fraction of a stride period when a leg is in stance phase. Values of duty factor change from 0 to 1. A duty factor $\beta = 0$ means the jumping state for cockroaches, and $\beta = 1$ means the all legs of cockroaches are in contact with the ground. In our trials, we analyzed all six legs' duty factors as shown in Figure 12. For each leg, duty factors decreased as velocities increased. A linear relationship between speed and duty factor can be observed. Proportionality coefficients in identical pairs of legs are almost the same, and they have significant differences among different pairs.

The relationship between duty factor and velocity was obtained for front legs, middle legs and hind legs, as shown in equations (11a), (11b) and (11c), respectively.

$$v = -40.8^{*}\beta + 35\ cm\ s^{-1} \quad (0.42 \leq \beta \leq 0.73,\ N = 47) \quad (11a)$$

$$v = -35.7^{*}\beta + 36\ cm\ s^{-1} \quad (0.5 \leq \beta \leq 0.8\ ,\ N = 47) \quad (11b)$$

$$v = -24.5^{*}\beta + 25\ cm\ s^{-1} \quad (0.42 \leq \beta \leq 0.76,\ N = 47) \quad (11c)$$

Table 1 shows the duty factors of each pair of legs. The duty factor variations of the front and hind legs are small, ranging from 0.51 to 0.67, comparing to large variations of middle legs ranging from 0.58 to 0.74. The majority of the duty factors in samples are larger than 0.5, which means that the legs stay longer on the ground than in the air. There is an overlap between two support triangles. The overlap corresponds to a transitory period for the adjustment of body gesture and the transition of support polygons. This transitory period guarantees the flexibility and stability of the cockroaches especially at a high speed. In addition, duty factors of the middle legs are significantly larger than the front and hind legs, considering the support triangles, the middle legs of

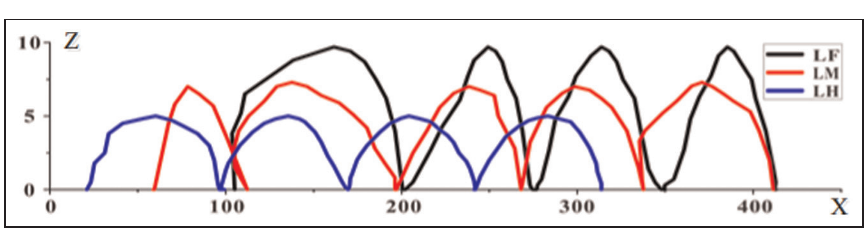

Figure 10. Vertical two-dimensional trajectories of three left leg-ends of cockroach's flat walking (x axis unit: pixel; z axis unit: mm).

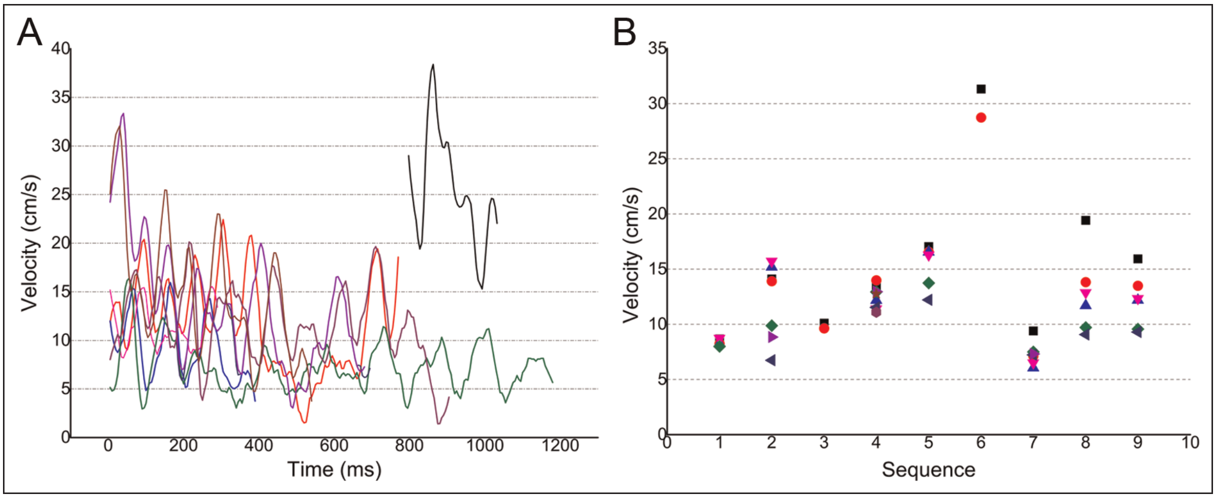

Figure 11. (A) Instantaneous velocity of continuous movement of nine sequences. (B) Mean stride velocity of nine sequences.

Table 1. Statistics of duty factor.

	N	Mean	Deviation	Minimum	Median	Maximum
Front	47	0.594	0.073	0.42	0.59	0.73
Middle	47	0.66	0.078	0.5	0.675	0.8
Hind	47	0.586	0.081	0.42	0.58	0.76

cockroaches provide more support force. In a stride, a larger duty factor of the middle legs stands for a longer time to support the body, which provides the cockroach with better stability.

Stride frequency (f) is defined as the amount of strides in unit time, which shows the transition frequency of swing and stance phase. In our analysis, stride frequency was calculated by computing reciprocal of stride period. Figure 13 shows the relationship of mean velocity and stride frequency in all steps. It can be seen that the stride frequency increases linearly with velocity, ranging from 3 to 8 Hz, while the average frequency is found as 5.63 ± 1.29 Hz for the 47 cockroaches as whole.

Stride length (l) is defined as the distance between two contiguous footprints of one leg, and it can also be considered as displacement of leg-ends during swing phase. Stride length consists of two parts: displacement of coxa, and relative stride length (l_R). Relative stride length is defined as the distance of leg-end relative to its coxa. In our trials, the relative stride length was calculated by subtracting the displacement of the COM from displacement of the leg-end in the swing phase. Table 2 lists stride length statistics of three pairs of legs. Mean stride lengths of the front and middle legs were almost the same, and both were larger than that of hind legs (the difference was less than 5%). The relative stride lengths in each pair of legs are listed in Table 3. It can be noticed that there were remarkable differences in the relative stride lengths among three pairs of legs. The middle legs have a relative stride length about 12.23 ± 2.38 mm, which is much longer than that of the front and hind legs. The smaller displacement of coxa of middle legs in swing phase may account for the difference.

Coordination among different legs

The coordination of each leg, the gait, is an important characteristic of legged animals. Hughes studied locomotion of hexapod insects such as *Periplaneta*, *Blatta*, and *Carabus*, and summarized that the most common gaits of hexapod insects was tripod gait (Hughes, 1952). While moving with tripod gait, insects alter two triangles to support their bodies, and each support triangle consists of an ipsilateral front and hind leg and a contralateral middle leg.

In our trials, two sequences were analyzed to study the gait patterns of *Blaptica Dubia*. In Figure 14, two gait patterns were shown together with the corresponding instantaneous velocity diagrams. Figure 14(A) shows the sequence with fast walking, whose mean stride velocity is about 30 $cm\ s^{-1}$, compared with a slow walking with a mean stride velocity about 7 $cm\ s^{-1}$ shown in Figure 14(B). The cockroach *Blaptica Dubia* adopted the tripod gait in free walking as seen from the observation results. However, some differences between two sequences can be noticed: during the first stride of fast walking, there was a short period that only two legs support the body, which indicates dynamic walking, as instantaneous velocity was larger than 20 $cm\ s^{-1}$.

Local extreme values of instantaneous velocity curves are marked in both figures, together with corresponding moment in a stride. The moment when extreme velocities are reached could further show the locomotion behavior of cockroaches. While the subject moves fast, the instantaneous velocity reaches to a minimum slightly after a new supporting triangle is taken into action, while it reaches to a maximum before the

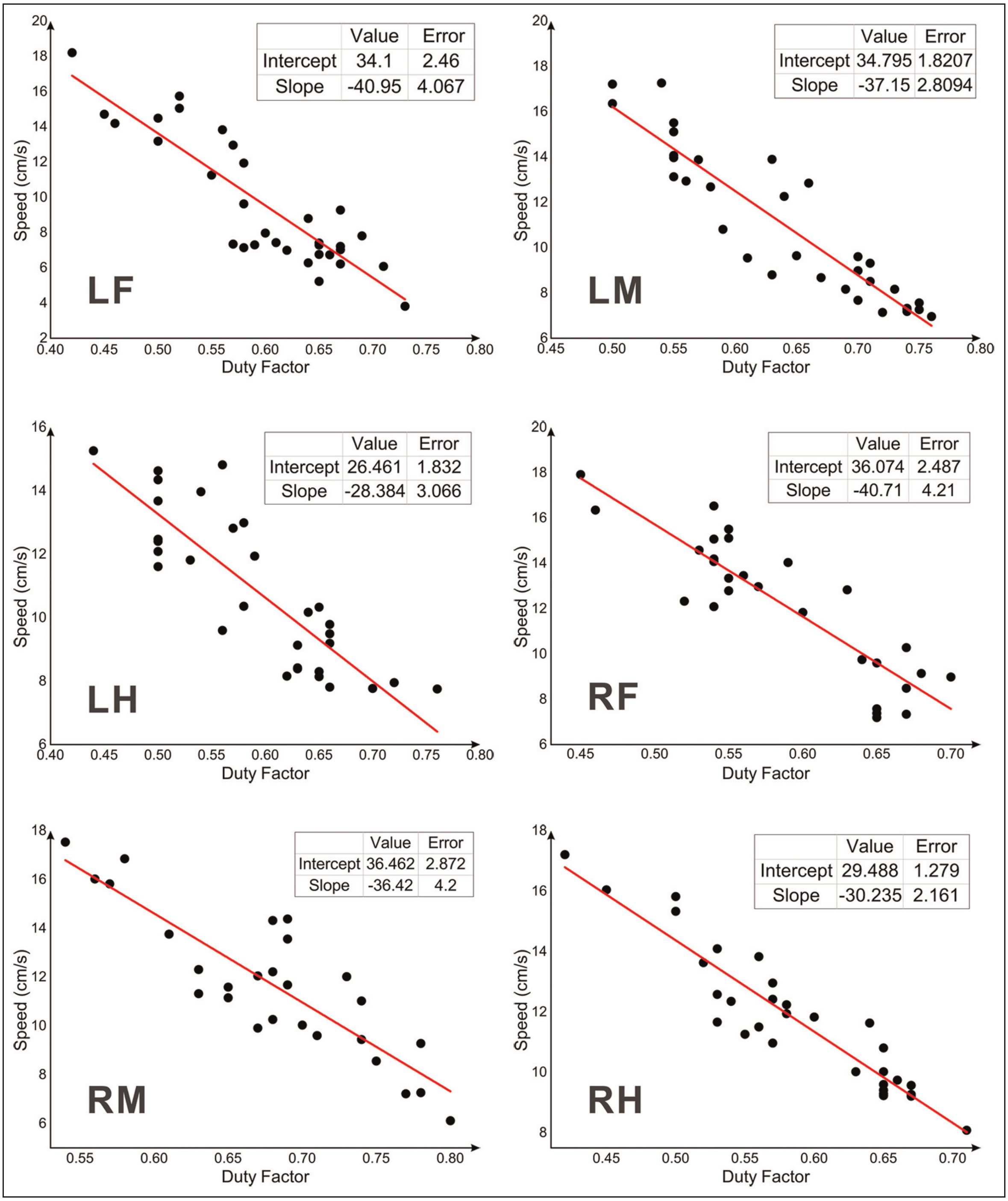

Figure 12. Mean stride velocity as a function of duty factor of each leg in the cockroach. Velocity decreased almost linearly with duty factor increasing. For legs of a pair, the slope and intercept parameters are similar, for different pairs, the differences of parameters are remarkable.

Table 2. Statistics of stride length (mm).

	N	Mean	Deviation	Minimum	Median	Maximum
Front	47	19.38	3.45	9.42	19.8	28.2
Middle	47	19.23	3.52	10.25	20	25.83
Hind	47	18.54	2.73	11.42	18.95	26.1

Table 3. Statistics of relative stride length (mm).

	N	Mean	Deviation	Minimum	Median	Maximum
Front	47	10.78	2.49	6.86	10.13	19.49
Middle	47	12.23	2.38	6.79	12.87	15.93
Hind	47	9.97	1.92	6.56	9.84	17.55

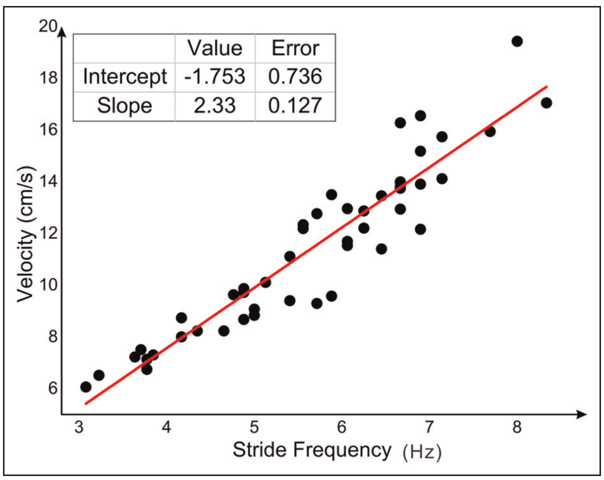

Figure 13. Mean stride velocity as a function of stride frequency in the cockroach.

supporting phase of this triangle is over. On the other hand, for slow movements, the velocity reaches generally to a maximum at the middle of a stride, while it reaches to a minimum at the end of an overlap phase.

Implementation of a hexapod walking robot

A major purpose of biology observation of insects is to understand the internal mechanism of their locomotion. The obtained data are then provided and used into the design and building of hexapod robots. A walking robot was designed and constructed to incorporate useful principles of biological locomotion.

The degrees of freedom of front legs, middle legs and hind legs in a cockroach are five, four, and three, respectively. The length proportion of hind legs measured from biological observation is 6:8:17. Unlike cockroaches, the hexapod robot has six identical legs. Each leg contains three linkages, which can be considered as coxa (41 mm), femur (60 mm), and tibia (123 mm) in the natural counterpart, respectively. The tarsus is ignored in the current design, and replaced by a spring system to substitute part of the function of tarsus, i.e., absorbing the impact force during touchdown on the ground. Besides, it has a low COM to enhance the stability and an additional body joint to improve the performance of climbing.

The biological data is partially transferred to practical robot platform, as shown in Figure 15. First, we extracted movement data from our experimental platform and analyzed the relative trajectories of leg-ends in Figure 15(A) which

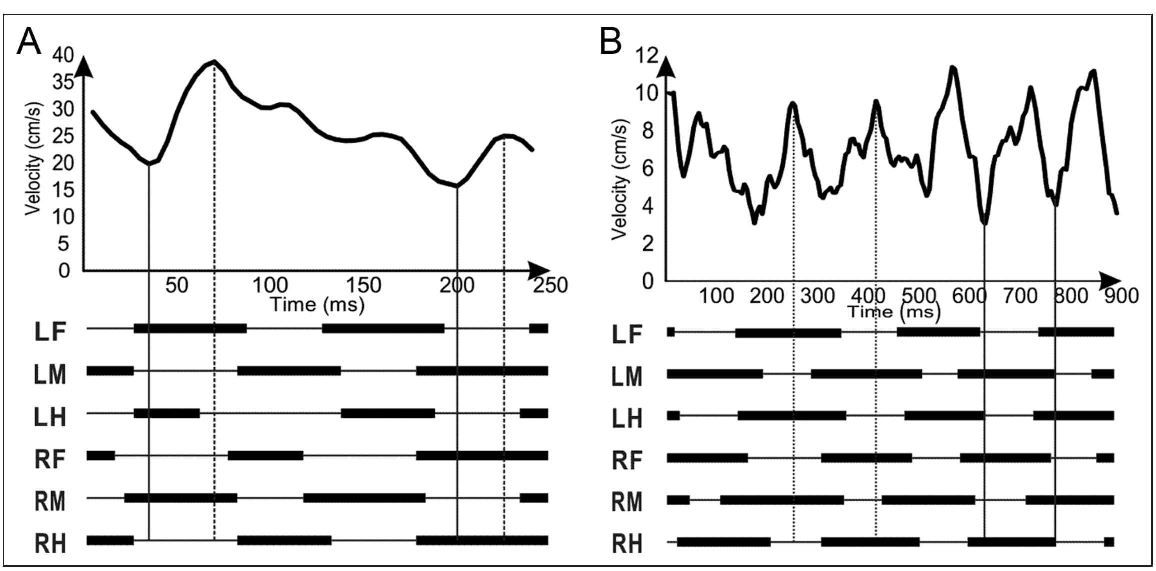

Figure 14. Gait patterns at different velocities. (A) Gait pattern at stride velocity of about 30 $cm\ s^{-1}$. (B) Gait pattern at stride velocity about 7 $cm\ s^{-1}$.

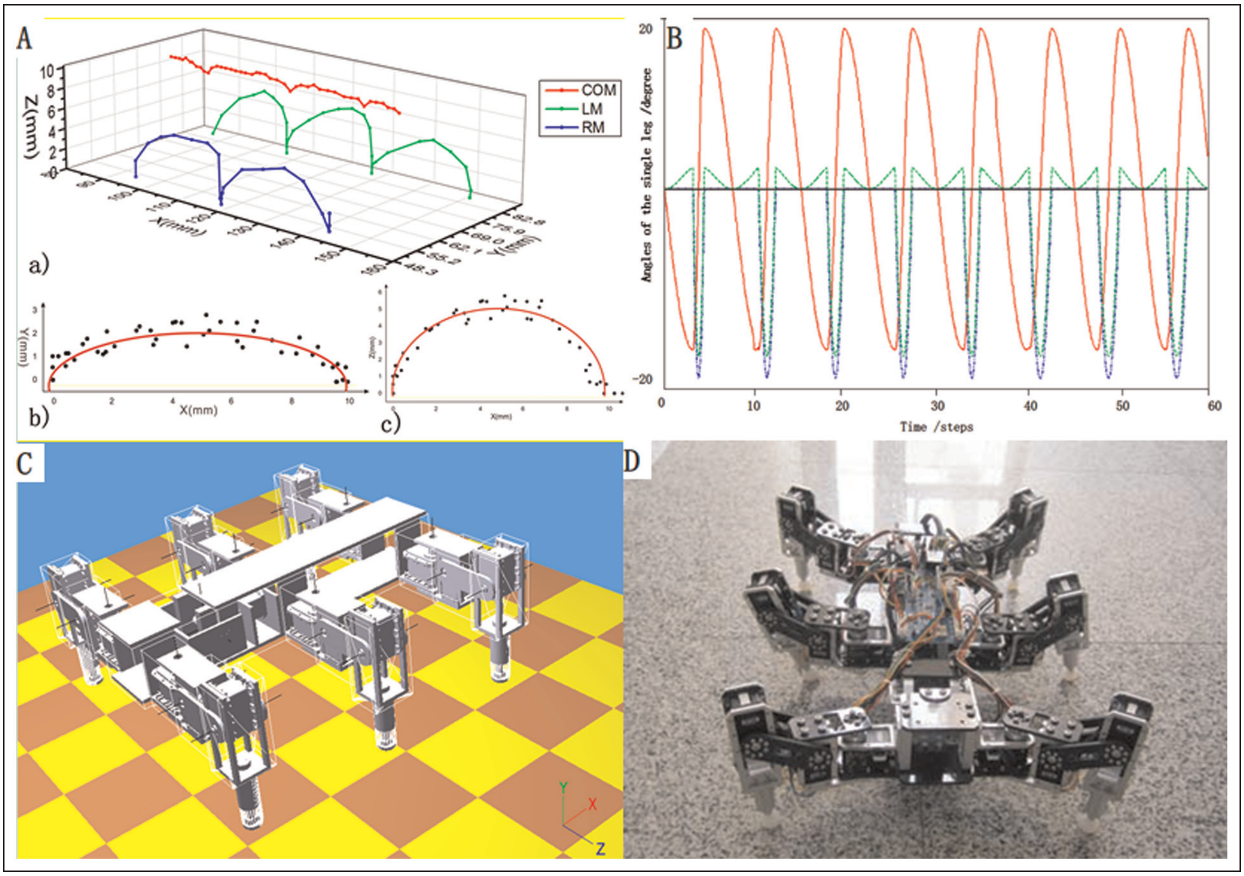

Figure 15. Linking insect walking to hexapod robots. (A) Data from locomotion observation of cockroaches. (B) Joint angles of single leg. (C) Simulation platform, modeled in Webots to verify the algorithm; (D) Hexapod robot prototype.

includes a) Three-dimensional trajectories of the COM; b) The projection of relative trajectories of leg-ends of hind legs at the x-y plane; and c) The projection of relative trajectories of leg-ends of hind legs at the x-z plane. The inverse kinematics is calculated to transform the trajectories into joint space (Chen et al., 2014) in Figure 15(B) where solid red line represents the angles of the thoracal-coxal joint, dashed blue line represents the angles of the coxal-trochanteral joint, and dotted green line stands for the angles of the femoral-tibial joint. So far, two platforms are available, including a simulation model in Webots and a physical prototype that was designed and manufactured.

Some measurements including COM, stability margin, velocity, joint angles, gaits, and walking patterns were obtained with the hexapod walking on a treadmill, as shown in Figure 16.

In the treadmill tests, the maximal moving speed of the hexapod (tripod gait) was 15 cm/s. Figure 17 shows four common gaits represented by the angles of the thoraco-coxa (TC) joint. They are wave gait (a), tetrapod gait (b), transition gait (c), and tripod gait (d), respectively. In the figures, dashed yellow lines, dotted dark lines, and solid green lines represent the right hind leg, the right middle leg, and the right front leg, respectively. In addition, solid blue lines, dotted red lines, and dashed prunosus lines stand for the left hind leg, the left middle leg and the left front leg, respectively.

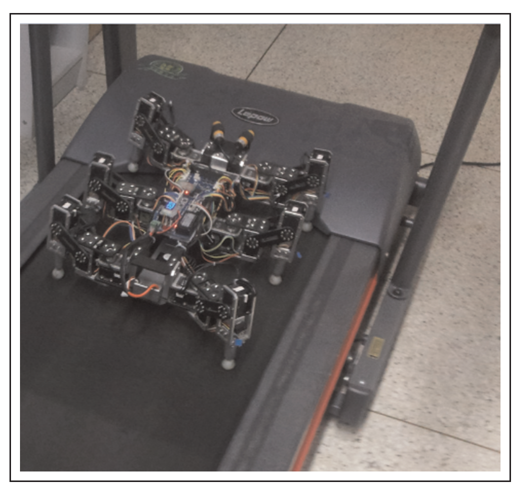

Figure 16. Treadmill tests.

Discussion

The new method was developed with an aim to improve the efficiency of data analysis in locomotion study. In this work, the method was applied to the locomotion study of

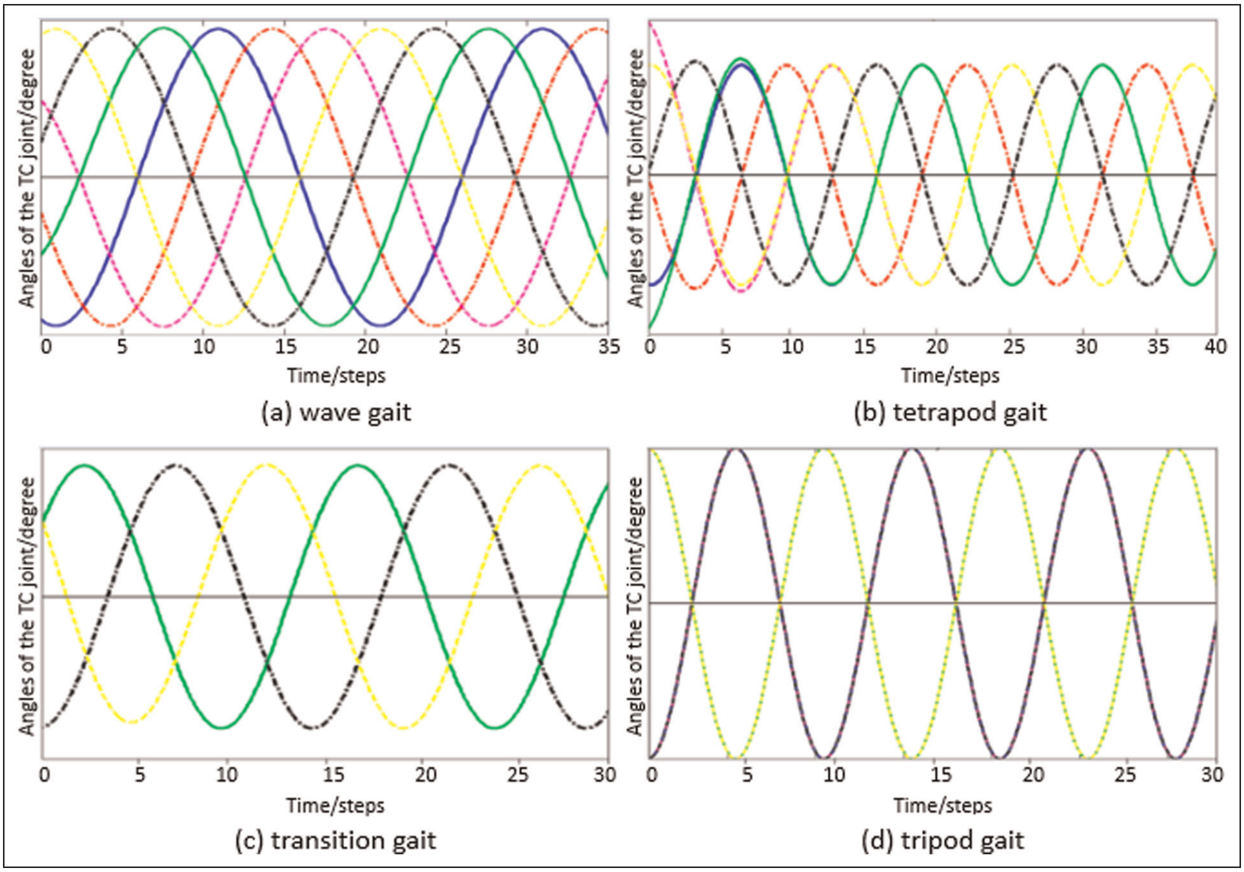

Figure 17. Four common gaits of the hexapod.

cockroaches. We also discuss briefly the method and the results, as presented below.

3D motion tracking with a single camera

The basic method which is commonly used in locomotion observation is to collect images by a high-speed camera and manually select the key points in each frame. As mentioned at the beginning of the paper, this process is often a laborious, time-consuming, and error-prone task. Here, we made an improvement by the proposed method to make the results more objective and accurate, which saves labor and time. A comparison between the manually-operated technique and the newly developed image processing-assisted method was made. In the comparison, we repeatedly handled a typical movement sequence (6 strides, 236 frames, and 3,540 points), using both manually extracting method and the proposed image processing method. It took a skillful investigator on average 120 min to fulfill this task, with 12 min for initialization and 1˜2 s to extract a single point. Compared to 2 man-hours by manual processing, only 0.2 man-hours was used in initialization by human, in addition to 5 min of computer time with our automated method. In other words, the proposed method saves 90% of the labor and achieves nearly the same accuracy.

Another improvement of the system is that only one camera used to obtain 3D motion information. Comparing with other systems where at least two sets of high-speed camera used (Bai et al., 2000), our system reduces the cost in equipment.

It is noted that the image processing algorithm is actually a hybrid method (manual initial processing and program assisted processing). Once the range of legs go over the value of displacement set in program, incorrect identification would appear, which would lead to wrong position data of the marker in the following frames. In order to correct the wrong data, it requires modify some parameters in corresponding program. Further improvement of the algorithm is considered for more efficient and accurate data processing.

Velocities and behaviors

Approaching to favorable stimulus and avoiding the harms is a rule that widely exists in animal and human behaviors. Take the escape behaviors for example: slight stimulus lead the cockroach *Periplaneta Americana* to walk or turn, while strong stimulus lead the cricket *Gryllus Bimaculatus* to run away, and sometimes even show some behaviors like jumping (Tauber and Camhi, 1995). During our trials, to make the cockroach move forward, in some cases we had to stimulate the rump of specimen, which always led to an instantaneous great acceleration. The instantaneous velocity graphs in Figure 14(A) can explain the escape behavior. While stimulated, the specimen got a peak instantaneous velocity 40 $cm\ s^{-1}$ in a stride from static state.

Tending to walk slowly is another outstanding behavior of the cockroach *Blaptica Dubia*. From the instantaneous velocity plots, the bias could be easily found. While moving with high initial velocity, subject specimens would slow down after several strides, and afterwards move forward at an almost constant low speed. Above all, without stimulus, the specimens would quickly recover to walking behavior with a low speed about $11.37 \pm 3.2\ cm\ s^{-1}$. This behavior tendency might be the result of biological evolution, to save energy and adapt to the environment. The observation agrees with some hypothesis such as trotting gaits for escape response, ambling gaits for exploring and foraging, and even slower locomotion to be intermittent (Reilly et al., 2007).

Gait patterns

Hughes and Deleomyn's research had shown that the cockroach characteristically used a tripod gait (Delcomyn, 1971: Hughes, 1952). This is also what we observed in the experiments, although there were remarkable velocity differences among sequences. Moreover, remarkable gait pattern differences were found between fast and slow walking.

Attempts to further divide the triple gait have been made by researchers. Graham divided the tripod gait of *Carausius morosus* into low- and high-speed walking based on the delay between front and hind legs on the left side (Graham, 1972). Bender studied the cockroach *Blaberus discoidalis* and divided tripod gait into trotting and ambling based on the stride frequency (Bender et al., 2011). In this work, a large amount of movement data has been analyzed about the differences between high-speed running and low-speed walking. According to the areas to traverse, the cockroach *Blaptica Dubia* uses trotting at a high speed and the ambling gait at a low speed, respectively. While the cockroach moves at a lower speed, transitory periods with six legs in supporting can be observed, and vice versa.

Comparison with related works

A description of locomotion in cockroaches was given by Hughes (1952), including the movements of the individual legs and several gaits. However, the experimental results presented were in general qualitative ones, by means of films taken at speeds of 16–32 frames/sec. Similar findings were reported in Delcomyn (1971), with a high-speed motion picture at 200 or 500 frames per second. Results in both works were obtained by counting the number of frames and manually extracting the marker points, which lead to relative low efficiency, compared to the proposed image processing assisted method. Vertical and horizontal ground reaction forces were measured using a miniature force platform, and the gait was defined by measuring ground reaction forces and mechanical energy fluctuations in Full and Tu (1990). In the study by Bender et al. (2011), walking speeds of cockroaches were explored in a large arena and three-dimensional limb and joint kinematics were extracted. Compared with these two groups, we constructed a different experimental platform, using only one high-speed camera and mathematical modeling method to fulfill the locomotion measurement to save the cost.

Conclusion and future work

In this work, an image processing algorithm was developed for efficient processing of high-speed camera recordings of cockroach locomotion. The algorithm can identify and track efficiently the points of interests on the specimen in locomotion, thus makes it possible to process large amount of locomotion recordings. Moreover, the algorithm is able to provide us the three-dimensional information of locomotion at insect-leg level, with a simple setup with one high-speed camera only. With the experiment platform built, locomotion observation and analysis were conducted for cockroaches. The results show that the proposed image processing algorithm improves the efficient and accuracy of experiments, and demonstrate the feasibility of the proposed method.

While the system has demonstrated its feasibility and efficiency, it can be further improved by including algorithms to automatically identify points of interest, without manual initialization. Moreover, the development can include the conversion from motion data to the location parameters for an easy use of the system. With the improvement of the method, more applications, in addition to the observation of cockroaches, could be found. In addition, the measurement platform would be improved so that the data of more complex behaviors, e.g. climbing, omnidirectional walking, could be extracted and applied in our prototype platforms.

Acknowledgements

The authors acknowledge the efforts of the anonymous reviewers and their constructive comments for improving the manuscript.

Conflict of interest

The authors declare that there is no conflict of interest.

Funding

This work was supported in part by the National Natural Science Foundation of China under grant number 61175108, and in part by the Beijing Natural Science Foundation under grant number 4142033.

References

Altendorfer R, Moore N, Komsuoglu H, et al. (2001) RHex: A biologically inspired hexapod runner. *Autonomous Robots* 11(3): 207–213.

Bai S, Low KH, Guo W, et al. (2000) Kinematographic experiments on leg movements and body trajectories of cockroach walking on different terrain. In: *Proceedings of IEEE International Conference on Robotics and Automation*, pp. 2605–2610.

Bender JA, Simpson EM, Tietz BR, et al. (2011) Kinematic and behavioral evidence for a distinction between trotting and ambling gaits in the cockroach Blaberus discoidalis. *The Journal of Experimental Biology* 214(12): 2057–2064.

Cappozzo A, Della CU, Leardini A, et al. (2005) Human movement analysis using stereophotogrammetry: Part 1: Theoretical background. *Gait & Posture* 21(2): 186–196.

Chan JC, Leung H, Tang JK, et al. (2011) A virtual reality dance training system using motion capture technology. *IEEE Transactions on Learning Technologies* 4(2): 187–195.

Chen W, Ren G, Wang J, et al. (2014) An adaptive locomotion controller for hexapod robot: CPG, Kinematics and Force Feedback *Science China Information Sciences* 57(11): 1–18.

Clegg B (2007) *The Man Who Stopped Time: The Illuminating Story of Eadweard Muybridge-Pioneer Photographer, Father of the Motion Picture, Murderer*. Joseph Henry Press.

Cruse H (2002) The functional sense of central oscillations in walking. *Biological Cybernetics* 86(4): 271–280.

Cruse H and Bartling C (1995) Movement of joint angles in the legs of a walking insect, Carausius morosus. *Journal of Insect Physiology* 41(9): 761–771.

Daniel TL (1985) Cost of locomotion: Unsteady medusan swimming. *Journal of Experimental Biology* 119(1): 149–164.

Delcomyn F (1971) The locomotion of the cockroach Periplaneta americana. *Journal of Experimental Biology* 54(2): 443–452.

Dickinson MH, Farley CT, Full RJ, et al. (2000) How animals move: An integrative view. *Science* 288(5463): 100–106.

Drucker EG and Lauder GV (2000) A hydrodynamic analysis of fish swimming speed: Wake structure and locomotor force in slow and fast labriform swimmers. *Journal of Experimental Biology* 203(16): 2379–2393.

Fontaine EI, Zabala F, Dickinson MH, et al. (2009) Wing and body motion during flight initiation in Drosophila revealed by automated visual tracking. *Journal of Experimental Biology* 212(9): 1307–1323.

Fukunaga T, Kubo K, Kawakami Y, et al. (2001) In vivo behaviour of human muscle tendon during walking. *Proceedings of the Royal Society of London. Series B: Biological Sciences* 268(1464): 229–233.

Full RJ and Tu MS (1990) Mechanics of six-legged runners. *Journal of Experimental Biology* 148(1): 129–146.

Garcia E, Jimenez MA, De Santos PG, et al. (2007) The evolution of robotics research. *Robotics & Automation Magazine, IEEE* 14(1): 90–103.

Graham D (1972) A behavioural analysis of the temporal organisation of walking movements in the 1st instar and adult stick insect (Carausius morosus). *Journal of Comparative Physiology* 81(1): 23–52.

Harris C and Stephens M (1988) *A combined corner and edge detector*. *Alvey vision conference*, Manchester, UK.

Hermanson JW (2004) Principles of Animal Locomotion. *Journal of Mammalogy* 85(3): 584–584.

Hsieh ST (2003) Three-dimensional hindlimb kinematics of water running in the plumed basilisk lizard (Basiliscus plumifrons). *The Journal of Experimental Biology* 206(23): 4363–4377.

Hof AL, Gazendam MGJ, Sinke WE, et al. (2005) The condition for dynamic stability. *Journal of Biomechanics* 38(1): 1–8.

Höfling E and Renous S (2004) High frequency of pauses during intermittent locomotion of small South American gymnophthalmid lizards (Squamata, Gymnophthalmidae). *Phyllomedusa: Journal of Herpetology* 3(2): 83–94.

Holmes P, Full RJ, Koditschek D, et al. (2006) The dynamics of legged locomotion: Models, analyses, and challenges. *Siam Review* 48(2): 207–304.

Hughes G (1952) The co-ordination of insect movements in the walking movements of insects. *Journal of Experimental Biology* 29(2): 267–285.

Ijspeert AJ (2008) Central pattern generators for locomotion control in animals and robots: A review. *Neural Networks* 21(4): 642–653.

Jindrich DL and Full RJ (2002) Dynamic stabilization of rapid hexapedal locomotion. *Journal of Experimental Biology* 205(18): 2803–2823.

Kuo AD (2002) Energetics of actively powered locomotion using the simplest walking model. *Journal of Biomechanical Engineering* 124(1): 113–120.

Lafond D, Duarte M, Prince F, et al. (2004) Comparison of three methods to estimate the center of mass during balance assessment. *Journal of biomechanics* 37(9): 1421–1426.

Moeslund TB, Hilton A, Kruger V (2006) A survey of advances in vision-based human motion capture and analysis. *Computer Vision and Image Understanding* 104: 90–126.

Quinn RD, Nelson GM, Bachmann RJ, et al. (2003) Parallel complementary strategies for implementing biological principles into mobile robots. *The International Journal of Robotics Research* 22(3–4): 169–186.

Reilly S, McElroy E and Biknevicius A (2007) Posture, gait and the ecological relevance of locomotor costs and energy-saving mechanisms in tetrapods. *Zoology* 110: 271–289.

Ritzmann RE, Quinn RD, Fischer MS, et al. (2004) Convergent evolution and locomotion through complex terrain by insects, vertebrates and robots. *Arthropod Structure & Development* 33(3): 361–379.

Spence AJ, Revzen S, Seipel J, et al. (2010) Insects running on elastic surfaces. *The Journal of Experimental Biology* 213(11): 1907–1920.

Tauber E and Camhi J (1995) The wind-evoked escape behavior of the cricket Gryllus bimaculatus: Integration of behavioral elements. *Journal of Experimental Biology* 198(9): 1895–1907.

Ting LH, Blickhan R, Full RJ, et al. (1994) Dynamic and static stability in hexapedal runners. *Journal of Experimental Biology* 197(1): 251–269.

Wang Y, Wang JL, Zhang GJ (2009) A virtual multi-structure light system for measuring insect motion parameters. *Journal of Optoelectronics*. Laser, 2, 020.

Yin H, Chai Y, Yang SX, et al. (2011) Fast-moving target tracking based on mean shift and frame-difference methods. *Journal of Systems Engineering and Electronics* 22(4): 587–592.